



$P_{sw}$  - Switching loss of IGBT  
Where  $P_{on}$  and  $P_{off}$  are the turn on and turn off losses [6]. The turn on and turn off losses are obtained by multiplying the turn on and turn off energies provided in the device datasheet.

$$P_{sw} = (E_{on} + E_{off}) \times f_s \quad (2)$$

Where  $E_{on}$  and  $E_{off}$  are turn on and turn off energies and  $f_s$  is the switching frequency.

The conduction losses include the losses of the IGBT as well as that of the freewheeling diode.

$P_{con}$  - Total conduction loss

$$P_{con} = P_{IGBT} + P_{FWD} \quad (3)$$

$$P_{IGBT} = I_p \times V_{ce} \times \left( \frac{1}{8} + \frac{m_i}{3} \cos \theta \right) \quad (4)$$

$$P_{FWD} = I_p \times V_f \times \left( \frac{1}{8} - \frac{m_i}{3\pi} \cos \theta \right) \quad (5)$$

$P_{IGBT}$  - Conduction loss of IGBT

$P_{FWD}$  - Conduction loss of freewheeling diode

$V_{ce}$  - Saturation voltage of IGBT (from datasheet)

$I_p$  - Peak value of the load current

$V_f$  - Saturation voltage of the freewheeling diode (From datasheet)

$m_i$  - Modulation index

$\cos \theta$  - Load power factor.

From (4) & (5), it can be inferred that the conduction loss depends on the peak current and not the switching frequency. When the IGBT is turned on the freewheeling diode gets reversed biased and the recovery current flowing through it causes the recovery loss. This is expressed as:

$$P_{rr} = \frac{1}{8} \times I_{rr} \times V_{dc} \times T_{rr} \times f_s \quad (6)$$

$P_{rr}$  - Recovery loss

$I_{rr}$  - Reverse recovery current (from datasheet)

$T_{rr}$  - Reverse recovery time (from datasheet)

$V_{dc}$  - Dc link voltage

To calculate the losses analytically the curve tracing equations are derived by formulation the least square solution and third-degree approximation has been considered for better accuracy [7]. For the simulation purpose the IGBT datasheet CM1400DY24NF has been used and hence the equations have been computed for the same. The values of  $V_{ce(sat)}$ ,  $E_{sw(on)}$ ,  $E_{sw(off)}$ ,  $V_f$ ,  $T_{rr}$  &  $I_{rr}$  are calculated as a function of  $I_p$ . The loss for a single switch has been computed using (1-6) and the total losses are the sum of the losses for six switches.

$$V_{ce(sat)} = 0.6466 + 0.0016I_p - 5.1494 \times 10^{-7}I_p^3 + 8.9606 \times 10^{-11}I_p^3$$

$$E_{sw(on)} = 0.005 + 6.851 \times 10^{-5}I_p - 8.323 \times 10^{-9} \times I_p^2 + 9.32 \times 10^{-12}I_p^3$$

$$E_{sw(off)} = 0.0082 + 1.942 \times 10^{-4}I_p - 7.55 \times 10^{-8} \times I_p^2 + 2.58 \times 10^{-11}I_p^3$$

$$V_f = 0.7222 + 0.0017I_p - 5.6354 \times 10^{-7}I_p^2 + 1.0667 \times 10^{-10}I_p^3$$

Using these equations, the datasheet parameters have been computed as a function of the load current. For the simulation studies the Thermal Module in PSIM has been used which is a good tool for estimating and analyzing the power losses [8]. The basis for this is the Device Database Editor which allows the user to add new devices to the data base and manage them with ease. The devices are saved in the directory in which PSIM is installed and while simulating, these devices can be used from the database. The behavior model of the device is used in the simulation. It takes into account static characteristics like conduction voltage drop and on state resistance but not the dynamic characteristics. Based on the voltage, current and the junction temperature values from simulation, PSIM accesses the device database and calculates conduction and switching loss. The results depend upon the accuracy of the device data as well as proper scaling of the results from actual operating conditions. The device manufacturer provides the loss simulator for estimating the losses and thereby the junction temperature. In Mitsubishi devices the loss simulator available is Melcosim through which the losses have been estimated [9]. The parameters which are taken into account are current, dc link voltage, modulation index, power factor, switching frequency and supply frequency. These are the primary parameters which influence the loss. The switching method used to calculate the loss is the SPWM for the three-phase inverter.

### III. MODULATION TECHNIQUES

#### 1. Space Vector Modulation

The space vector modulation technique offers advantages over the SPWM in terms of the dc bus utilization and the harmonic spectrum. Hence this technique is widely used in various applications. This technique is based on the eight switching combinations of the three phase two level inverter [15]. These eight switching states give rise to Space Vector diagram shown in figure 3.

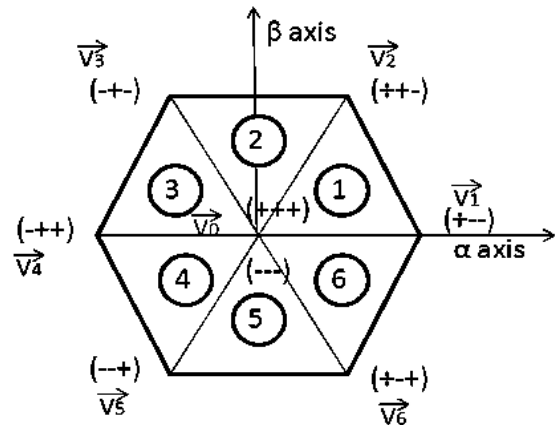


Fig.3. Space Vector diagram

The zero switching states are at the center and six active vectors form the hexagon. The six active vectors form the sectors and

switching takes place such that the nearest vectors are switched to generate the required output vector. The three-phase system is analyzed as a whole as the Clarke's transformation is applied which leads to the switching as a combined effect of all the three phases.

The Volt second balance principle is used to calculate the timings where the product of the reference and sampling period equals the sum of volt multiplied by the time interval of the chosen space vectors. The maximum output voltage in the linear range is  $0.707 V_{dc}$  which is 15.5% more than SPWM. Also, by designing the zero-vector placement different switching sequences can be created, which contributes to new switching techniques.

## 2. Sinusoidal Pulse Width Modulation

In the SPWM technique to produce the balanced three phase output voltages the triangular wave is compared with three references which are  $120^\circ$  apart [16]. The carrier wave frequency is higher than the reference which is at supply frequency. The frequency modulation ratio  $m_f$  is defined as:

$$M_f = f_s / f_1 \quad (7)$$

$f_s$  - Frequency of the carrier  
 $f_1$  - The supply frequency  
 The amplitude modulation ratio (modulation index) is defined as:

$$M_i = \text{reference} / \text{Carrier} \quad (8)$$

The dc component present in the phase voltages being similar is cancelled out in the line-to-line voltages. Due to this pattern of the line-to-line voltages the harmonics are absent at the carrier frequencies and appear as sidebands of the switching frequencies and their multiples. In linear modulation range ( $0 \leq m_i \leq 1$ ) the maximum line-to-line voltage available is  $0.612 V_{dc}$ .

## 3. Hybrid PWM (HPWM)

HPWM strategy, [12], is based on the clamping of one modulation signal for sometime during the non-common intervals between DSPWM and SPWM. As the modulation signals are clamped to zero for an additional time, switching frequency of the power switches is reduced and switching losses also decrease. The exact combination is chosen by a sharing variable, which can take values within the interval [0; 1] When the parameter D takes the extreme values zero or one, the HPWM becomes DSPWM or SPWM, respectively. Figure 4 shows that, when the modulation signal from SPWM crosses zero, the absolute value of the DSPWM modulation signals are exactly half the modulation index ( $m = \text{amplitude of the modulation signals}$ ). This condition is used to determine the extension of the common interval directly from the instantaneous values of the modulation signals obtained from DSPWM. The modulation signals are compared with the value of  $x=D (m/2)$  to determine the additional intervals in which these signals need to be clamped to extend SPWM patterns further.

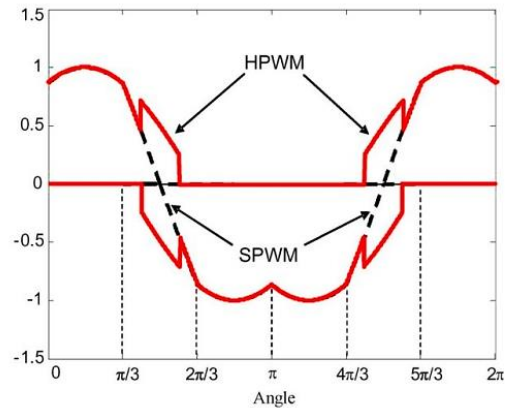


Figure 4. Modulation signal for HPWM

## CONCLUSION

Even though the generation of SVM technique is different compared to SPWM both are regularly sampled algorithms and both create switched output waveforms to produce the result. Both the techniques have the similar switching pattern. In SPWM the nearest vectors are automatically selected whereas in SVM the switching sequence is designed by the user. The only difference in these two techniques is the placement of the zero vectors. In SPWM the sequence is automatically generated whereas in SVM it can be designed. Conventional SVM implementation centers the active space vectors in each half carrier period and splits the remaining zero space vector time equally between which is shown in figure 3. From the sequence we can see that the sequence of the space vectors reverses over a complete carrier interval which is also the case with SPWM.

## References

- [1] D.Grahame Holmes and Thomas.A.Lipo, "Pulse Width Modulation for Power Converters – Principles and Practice," IEEE Press, Wiley Interscience New York, 2003, pp 259-335.
- [2] "IGBT MOD & IntelliMOD –Intelligent Power Modules," Applications and Technical databook, 1994.
- [3] Ahmet Hava, Russel Kerkman and Thomas A Lipo, "A HighPerformance Generalized Discontinuous PWM Algorithm," IEEE Transactions on Industry Applications vol 34 No 5 September/October 1998.
- [4] "Space Vector with Quadrature Control," – Application note, Texas instruments.
- [5] Bin Wu, "High - Power Converters and AC drives," The Institute of Electrical and Electronics Engineers, Inc., 2006, pp 95-118.
- [6] Jun-ichi Itoh, Takumi Ogura, "Evaluation of total loss for an inverter and motor by applying modulation strategies," 14th International Power Electronics & Motion Conference EPE PEMC 2010.
- [7] Ankit G Patel, "Estimation of IGBT Junction Temperature using DSP to display it on VVVF inverter drive screen," Dissertation submitted to faculty of Technology & Engineering ,M S University, Vadodra, May 2011
- [8] User's Guide-PSIM, Version 9.0, January 2010.
- [9] Power loss Simulation software-User Manual, Power Device Works, Mitsubishi Electric, April 2010

- [10] J. Pou, J. Zaragoza, P. Rodríguez, S. Ceballos, V. Sala, R. Burgos, and D. Boroyevich, "Fast-processing modulation strategy for the neutral-point-clamped converter with total elimination of the low-frequency voltage oscillations in the neutral point," *IEEE Transactions on Industrial Electronics*, vol. 54, no. 4, pp. 2288–2299, Aug. 2007.
- [11] J. Zaragoza, J. Pou, S. Ceballos, E. Robles, P. Ibaez, and J. L. Villate, "A comprehensive study of a hybrid modulation technique for the neutral-point-clamped converter," *IEEE Transactions on Industrial Electronics*, vol. 56, no. 2, pp. 294–304, Feb. 2009.
- [12] J. Zaragoza, J. Pou, S. Ceballos, E. Robles, C. Jaen, and M. Corbalan, "Voltage-balance compensator for a carrier-based modulation in the neutral-point-clamped converter," *IEEE Transactions on Industrial Electronics*, vol. 56, pp. 305–314, Feb. 2009.
- [13] R. Maheshwari, S. Munk-Nielsen, S. Busquets-Monge, "Neutral-point current modeling and control for Neutral-Point Clamped three-level converter drive with small DC-link capacitors", in *Proceedings of the 2011 IEEE Energy Conversion Congress and Exposition (ECCE)*, pp. 2087–2094, Sept. 2011.
- [14] J. Pou, "Modulation and control of three-phase PWM multilevel converters," *Thesis Doctoral*, Universitat Politècnica de Catalunya, Nov. 2002.
- [15] X. Yuan, H. Stemmler, I. Barbi, "Investigation on the clamping voltageself-balancing of the three-level capacitor clamping inverter," in *Proceeding of the 30th Annual IEEE Power Electronics Specialists Conference*, vol. 2, pp. 1059–1064, 1999.
- [16] J. Shen, S. Schröder, R. Rösner, S. El-Barbari, "A comprehensive study of neutral-point self-balancing effect in neutral-point-clamped threelevel inverters," *IEEE Transactions on Power Electronics*, vol. 26, pp. 3084–3095, Nov. 2011.